PEG-modified Copper Cysteine for Photodynamic Therapy in Alzheimer's Disease

Zhihao Ma (mazhihao0622@163.com)
Jiangsu University, Zhenjiang
Chenglong Song
Jiangsu University, Zhenjiang
Kaitong Yang
Jiangsu University, Zhenjiang
Jie Wang
Jiangsu University, Zhenjiang

Research Article

Keywords:

Posted Date: March 15th, 2022

DOI: https://doi.org/10.21203/rs.3.rs-1446266/v1

PEG-modified Copper Cysteine for Photodynamic Therapy in Alzheimer's Disease

Zhihao Ma, Chenglong Song, Kaitong Yang, Jie Wang*

Institute for Advanced Materials, School of Material Science and Engineering, Jiangsu University, Zhenjiang, 212013, China

Abstract

As a progressive neurodegenerative disease, Alzheimer's disease (AD) is characterized by the accumulation and misfolding of amyloid polypeptides (Aβ) which result in irreversible brain damages, cognitive decline and behavioral impairment. Photodynamic therapy (PDT) has received much attention as a potential approach for AD treatment. In this study, we investigated a novel multifunctional theranostic photosensitizer, copper cysteine (Cu-Cy). By performing PEG modification on nanoparticles' surface, the particle size and cytotoxicity were significantly reduced. Under UV irradiation, Cu-Cy-PEG can produce reactive oxygen species (ROS) and could degrade Aβ(1-40) aggregates efficiently. This is the first case for Cu-Cy-PEG being used for degrading Aβ aggregates in vitro. The macroscopic amyloid aggregates were photodegraded by Cu-Cy-PEG into amorphous particles. This study firstly proved that Cu-Cy-PEG may serve as a potential treatment in AD therapy.

1. Introduction

Evidence showed that the β-sheet secondary structure of Aβ proteins leads to its self-assembly and amyloid deposites in brain, which caused neuron death and clinical symptoms[1-3]. Aβ proteins are produced by the hydrolysis of amyloid precursor protein (APP) by β-secretase and γ-secretase[4-6]. The most common species of Aβ in the human body includes Aβ(1-40) and Aβ(1-42). Herein, inhibiting the aggregation of Aβ is an important strategy for AD treatment.

PDT is a minimally invasive therapy which can be applied in the clearance of Aβ[7-9]. The PDT therapy requires three aspects: photosensitizer (PS), light irradiation and oxygen (O_2). However, traditional photosensitizers can cause cytotoxicity under light irradiation[10-12]. The biosafety of photosensitizers becomes a vital problem for PDT. As a new generation of PS, copper cysteine (Cu-Cy) has better physical stability and biocompatibility. Because of its ability of emitting strong fluorescence, it may be a good choice for drug delivery in deep tissues[13]. Compared with traditional materials, Cu-Cy can produce reactive oxygen species (ROS) in a wide range of light irradiation including UV and X-ray or microwave. The ROS could also be generated in the hydrolysis of Cu^+ which is employed to generate ROS as shown in Scheme 1[14]. The ROS was mainly of singlet oxygen($^1O_2$) which is able to destroy the secondary structure and efficiently degrade Aβ aggregates[15]. In addition, the researchers previously found that the presence of Cu^{2+} could prevent Aβ protein molecules from misfolding into β-sheet structure and forming senile spots[16]. In summary, theoretically, the Cu-Cy could antagonize the amyloydosis and reduce the existing fibrillar deposites in the brain. We try to test the potential treatment effect for Cu-Cy to degrade amyloid aggregates in Alzheimer's disease.

In this study, Cu-Cy with uniform particle size was synthesized successfully by thermal solvent method. The nanoparticles were further refined with the involvement of PEG-4000[17]. Finally, the degradation of pre-prepared Aβ(1-40) aggregates was performed by Cu-Cy-PEG under the irradiation of UV. (Scheme 1)

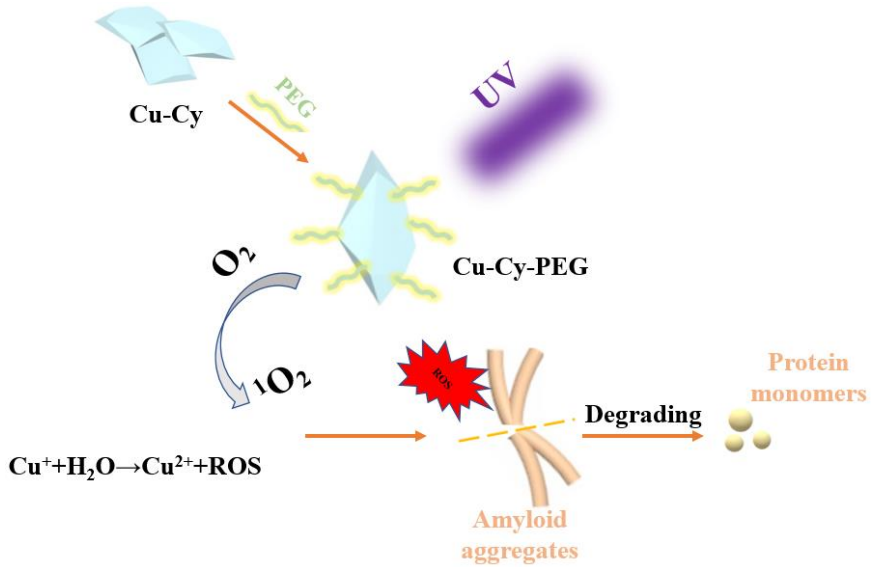

Scheme 1. The synthesis of Cu-Cy-PEG and the degradation of Aβ(1-40) aggregates under UV.

2. Experimental

2.1 Materials

All the reagents were purchased from Aladdin company (China) including $CuCl_2 \cdot 2H_2O$ (99.9% purity), cysteamine hydrochloride (98% purity), PEG-4000 (99% purity), sodium hydroxide (NaOH). 1,1,1,3,3,3-Hexafluoro-2-propanol(HFIP) was purchased from Sigma-Aldrich. Dimethyl sulfoxide (DMSO), fetal bovine serum (FBS) and dulbecco's modified eagle medium (DEME) were purchased from Biological Industries.

2.2 Synthesis of Cu-Cy-PEG

All the glass instruments were washed clean with aqua regia before use. 277mg $CuCl_2 \cdot 2H_2O$ was added to 50mL deionized water and magnetically stirred in a sealed three-neck flask until fully dissolved. 552mg cysteamine hydrochloride and 40mg PEG-4000 were added into the solution under the protection of nitrogen (N_2). Keep the circulation of N_2, 1M NaOH was used to adjust the pH to 7. Continuing to stir the solution at room temperature for 10min, and the color of solution turned into dark purple. Subsequently, the solution was heated to a boiling point and maintained for 15min. After cooling, the mixture was centrifuged at 12000rpm for 10min and washed for 3 times with a combination of water and ethanol (v:v=5:4). The final

products were obtained by drying in a vacuum at 40℃ overnight.

2.3 Preparation of Aβ(1-40) aggregates

To prepare 1mg/mL Aβ(1-40) solution, 1mg Aβ(1-40) powder was dissolved in 1,1,1,3,3,3-Hexafluoro-2-propanol (HFIP) and then put in a vacuum drying tank to remove HFIP and subsequently redissolved with 1mL water. After that, the Aβ(1-40) solution was incubated on a thermo mixer at 37℃ for 24h.

2.4 The measurement of $^1O_2$

Singlet oxygen sensor green (SOSG) is a sensitive probe to detect the presence of $^1O_2$. The prepared Cu-Cy-PEG solutions at different concentrations were exposed to UV light for 20min. After that, 0.1mM SOSG was added into the solutions after irradiation to attain an ultimate concentration of 1% (v/v). The fluorescence spectra were measured by ELASA at 525nm.

2.5 The measurement of ThT fluorescence

25μL of 1mM ThT solution and 25μL Aβ(1-40) aggregates were mixed with 100μL H_2O in a 96-well plate and measured by ELASA. The excitation light and emission fluorescence wavelengths are 450nm and 485nm, respectively.

2.6 Atomic force microscope (AFM) analysis

Sample preparation: 100μL of Aβ(1-40) aggregates was dripped in a climbing slice (NEST), and then dried at room temperature. All of AFM experiments were scanned on a SPM (Multi-Mode VIII, Bruker). The saved images all had a resolution of 512×512.

2.7 CCK8 assay

PC12 cells in cell experiments were derived from rat pheochromocytoma. The resuscitated cells were placed into the 1640 culture medium with 10% DEME, 10% FBS and 1% antibiotics. To ensure cell activity, the cells are re-cultured every two days. Then, 100μL of PC12 cell solution (105cells/mL) was added to each well and cultured at 37℃ with an atmosphere of 5%

CO_2 for 24h. Then the materials were added to co-culture with PC12 cells and after 24h 10μL CCK8 (Beyotime Biotechnology) was added into each wells. Finally, after 4h incubation, the results were measured by ELASA setting at 450nm.

3. Results and discussion

3.1 The synthesis and *characterization of the Cu-Cy*

The Cu-Cy was synthesized according to a previous report[18], the formula of Cu-Cy was $Cu_3Cl(SR)_2$ (R=$CH_2CH_2NH_2$). Most of $Cu_3Cl(SR)_2$ crystals are rectangular with the size ranging from about 3 to 10μm. Before characterizing the sample morphology, the aqueous solution of samples was centrifuged at 8000rpm for 10min to precipitate large particles. As shown in Figure S1a, the Cu-Cy nanoparticles were characterized by SEM and the morphology was consistent with previous reports[18,19]. In the absence of PEG modification, the Cu-Cy particle size was about 580nm shown in Figure S1b. In a contrast, with the adjunction of PEG-4000, as shown in Figure 1a-c, the SEM and TEM images indicated that the particle size of Cu-Cy-PEG was reduced to ~180nm and became more uniform as shown in Figure 1d. Accordingly, the color of the Cu-Cy solution changed from gray to clear and the dispersity in water was improved after PEG-4000 modification as shown in Figure S2.

As shown in Figure 1e, the XRD pattern of Cu-Cy-PEG showed a very sharp and intense peak which could indicate the high crystallinity of this material. The oxidation state of copper is Cu^+ instead of Cu^{2+}[20,21]. Because this is an entirely new compound, the measured XRD pattern couldn't match any Cu compounds in the current database. However, our result was coincident with a calculated one reported[22].

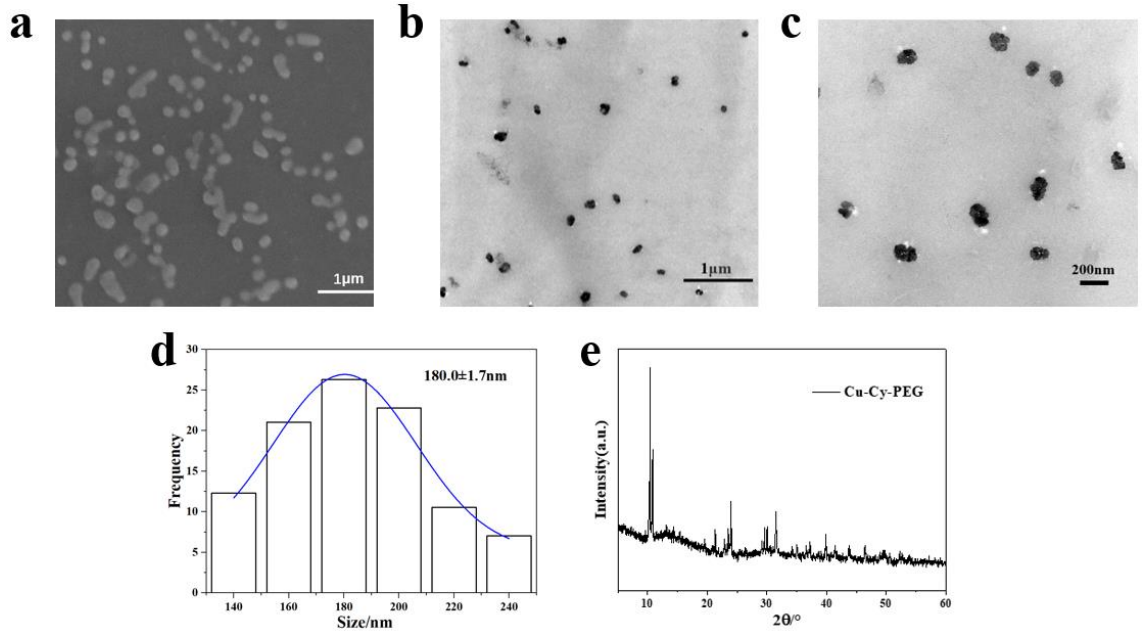

Figure 1. (a) SEM, (b,c) TEM images, (d) Size distribution and (e) XRD pattern of Cu-Cy-PEG

3.2 Characterization of optical properties

The UV absorption spectra as shown in Figure 2a had a distinct peak at 365nm. Being excited at 365nm, the fluorescence emission spectrum had a peak at 628nm which corresponded to the existence of Cu^{+}[23]. Many copper compositions can't emit light due to efficient internal conversion[24], but Cu-Cy-PEG in this study could emit a very strong orange fluorescence as shown in Figure 2c, and this fluorescence emission could last for about 5min. Thus, Cu-Cy-PEG is a multi-function material applied in both diagnosis and photodynamic therapy.

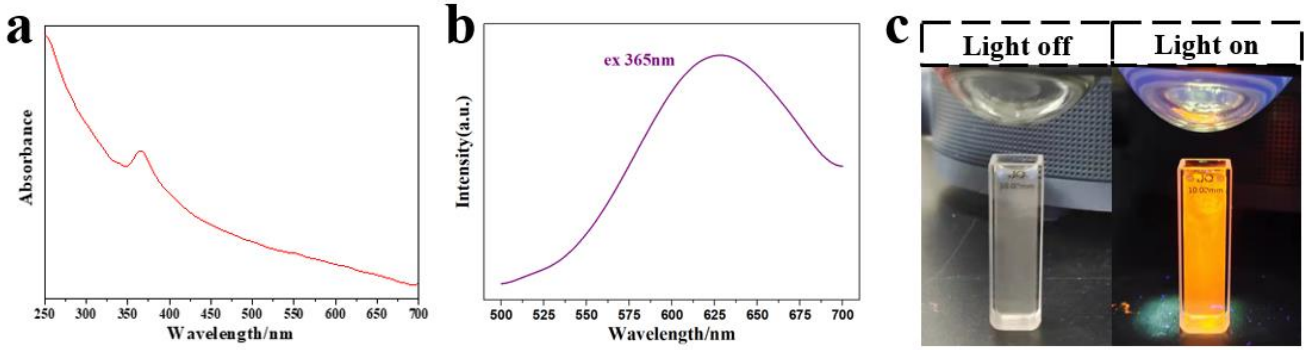

Figure 2. (a) The UV absorption spectra was measured by UV-2600i. (b) The fluorescence emission spectrum was measured by a Cary Eclipse Fluorescence Spectrophotometer (Agilent, Malaysia). (c) Comparison between light off (left) and light on (right).

Under the irradiation of UV, the system could produce different kinds of ROS such as $^1O_2$, ·OH and the main kind we focused on was $^1O_2$. By using SOSG as a trapping agent[25,26], emission

peaks at 525nm were measured with Cu-Cy-PEG of different concentrations. The fluorescence intensity showed a linear relationship with Cu-Cy-PEG concentrations, indicating that the output of $^1O_2$ was related to the change of Cu-Cy-PEG concentrations as shown in Figure 3b.

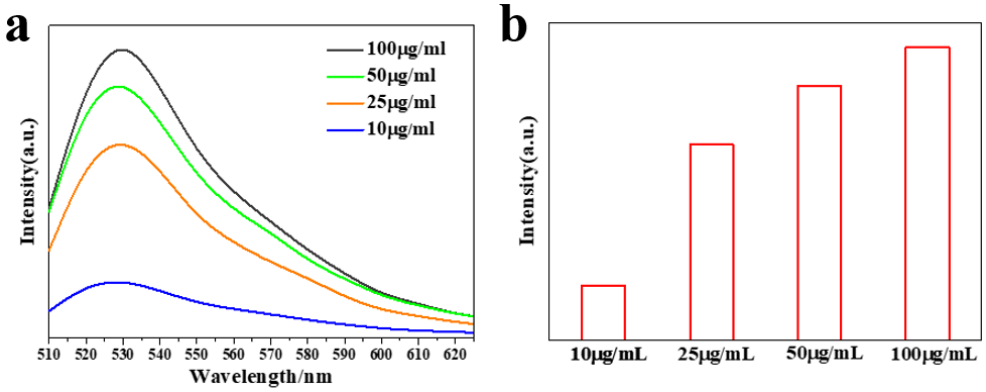

Figure 3. The fluorescence of Cu-Cy-PEG with different concentrations; (a) The fluorescence emission spectra of Cu-Cy-PEG at four concentrations (10, 25, 50, 100μg/mL) measured by ELASA; (b) fluorescence intensity of Cu-Cy-PEG with different concentrations at 525nm.

3.3 Cytotoxicity assay

The researchers found that Cu-cysteamine complexes have lower cellular dark toxicity due to the low leaching rate of copper ions[27]. In this study, we explored the toxicity on PC12 nerve cells induced by this material we synthesized. The results in Figure 3 showed an obvious comparison between Cu-Cy and Cu-Cy-PEG. When both of them were at low concentrations (10, 25μg/mL), cell viability of PC12 could maintain around 80%. As the concentration increased, the cytotoxicity of Cu-Cy multiplied sharply, for example, when the Cu-Cy concentration increased to 100μg/mL, the cell viability was weakened to 17%. In a contrast, the cell viability for 50 and 100μg/mL Cu-Cy-PEG could still reach 84% and 70%, respectively. Thus, the modification of PEG can not only improve the dispersion of nanoparticles in solution, but also significantly improve the biocompatibility.

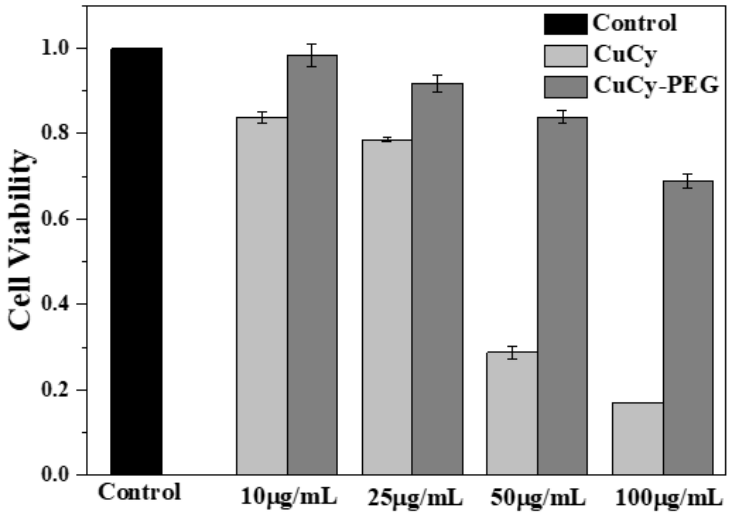

Figure 4. Cytotoxicity of PC12 cells incubated with Cu-Cy or Cu-Cy-PEG at different concentrations (10, 25, 50, 100μg/mL).

3.4 Disassembly of Aβ(1-40) aggregates by Cu-Cy-PEG

The capability of Cu-Cy-PEG for photodegrading Aβ(1-40) aggregates was comprehensively assessed. Firstly, the prepared Aβ(1-40) aggregates were verified by ThT assay. The self-assembly of Aβ(1-40) was monitored in a growth curve of ThT fluorescence shown in Figure 5a. The curve initially gradually rose and then staged into a steady state after about 800min. The morphology of Aβ(1-40) aggregates was scanned by TEM and AFM as shown in Figure 5b-c. It is the typical morphology that the dense fibrils shown in images tangled irregularly. Calculated by AFM height measuring of fibrils and statistics analysis, the height of Aβ(1-40) fibrils was 10.4±0.1nm as shown in Figure 5d.

According to the measurement of ROS and cytotoxicity of Cu-Cy-PEG, the concentration of 25μg/mL was chosen for degrading Aβ(1-40) aggregates due to its high output of $^1O_2$ and biosafety. Within the first 3 hours, both AFM and TEM images in Figure 6a-d showed that Aβ(1-40) aggregates decreased gradually with photodegradation went on. The height of aggregates dropped from 10.5nm to 5.1nm as shown in Figure 6e. It is worth mentioning that Aβ(1-40) aggregates were degraded into small particles when the time of photo-degradation reached 4 hours as shown in Figure 6f. The coverage ratio of aggregates in TEM images

changed from 60.2% of fibrils to 15% of degraded particles. It was a surprising result as previous materials couldn't degrade Aβ aggregates to such homogeneous protein monomers.

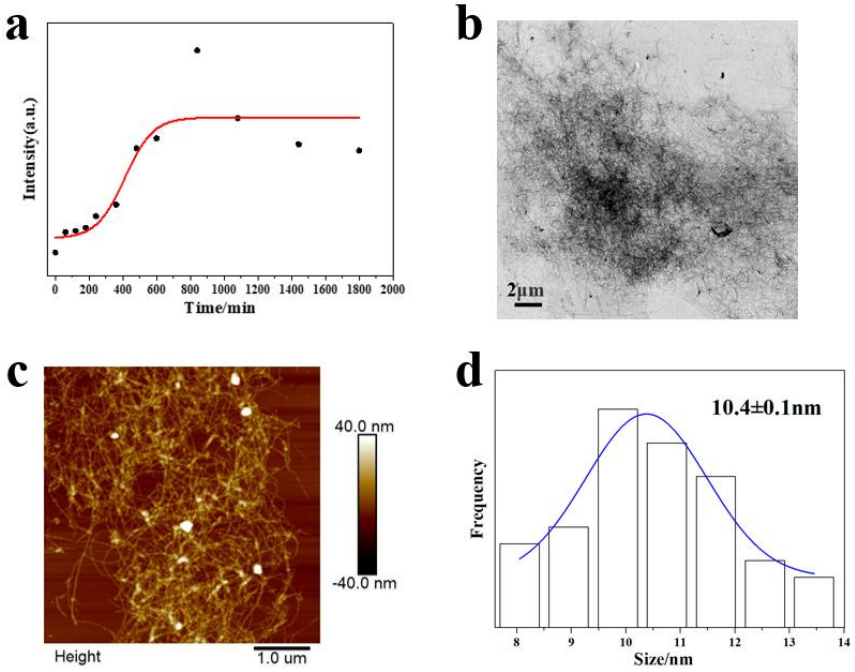

Figure 5. Aβ(1-40) aggregates was characterized by ThT assay, TEM and AFM. (a) Dynamic growth of Aβ(1-40) aggregates by ThT assay; (b,c) The morphology of aggregates characterized by TEM and AFM images; (d) Height distribution of Aβ(1-40) aggregates.

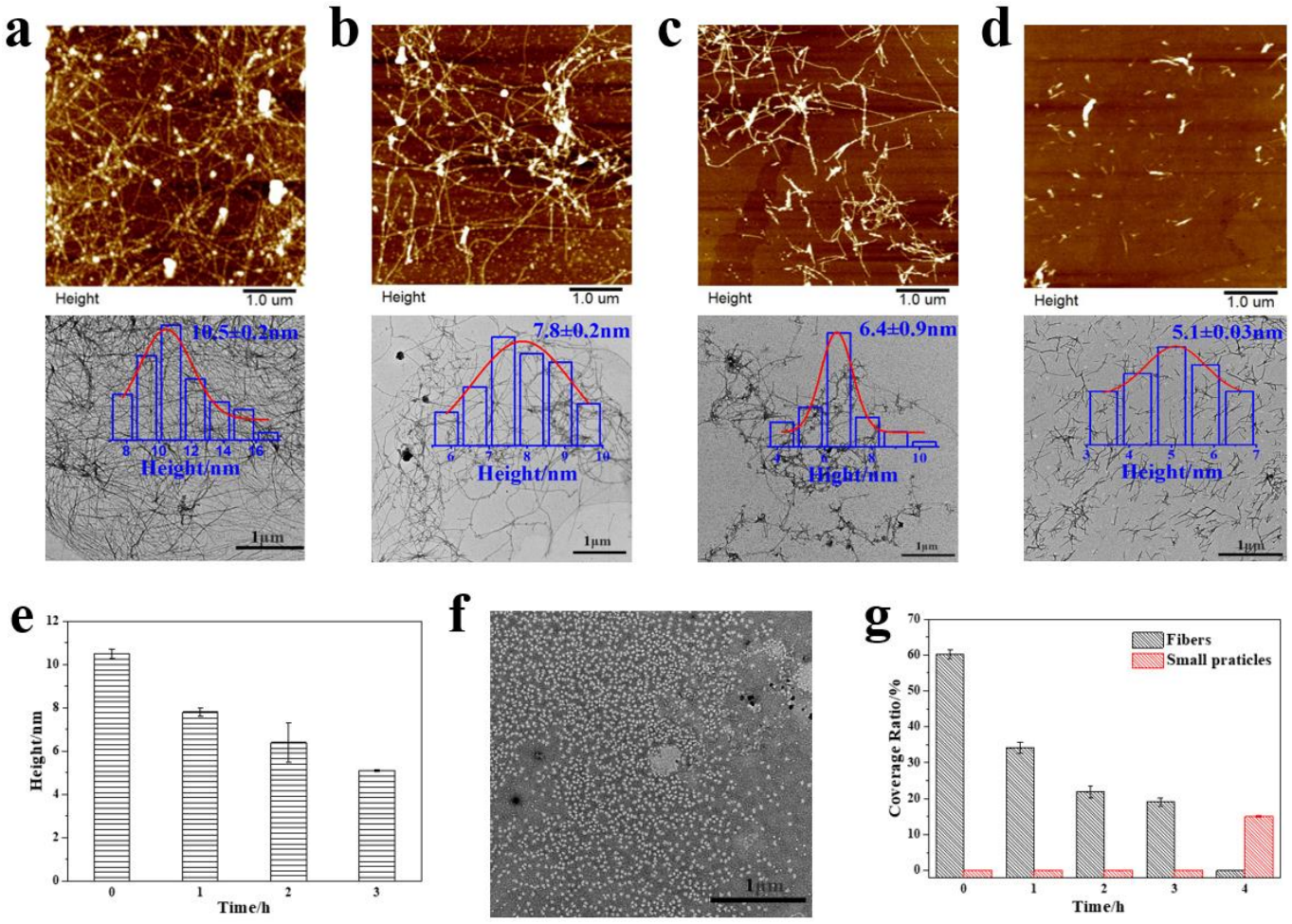

Figure 6. Disassembly of Aβ(1-40) aggregates by Cu-Cy-PEG. (a-d) The degrading of Aβ(1-40) aggregates was characterized by AFM, TEM and corresponding height analysis in the starting 3 hours (0, 1, 2, 3h); (e) Height distribution statistics of Aβ(1-40) aggregates; (f) TEM image of Aβ(1-40) aggregates after 4h degradation; (g) Coverage ratio statistics of Aβ(1-40) aggregates.

3.5 Secondary structure analysis in the process of degrading

Besides, the secondary structure change of Aβ(1-40) aggregates were characterized by Circular Dichroism spectra (CD) and ThT assay. As shown in Figure 7a, the CD spectra of 0h degradation showed a sharp peak at 195nm which represented the existence of β-sheet structure[28]. After an incubation with Cu-Cy-PEG, the typical peaks disappeared. Especially, after photodegradation for 1h, the intensity of CD spectra showed a significant decline as shown in Figure 7b. The result of ThT assay demonstrated that the photodegradation process was completed in about 4 hour which was consistent with the other characterizations in this study.

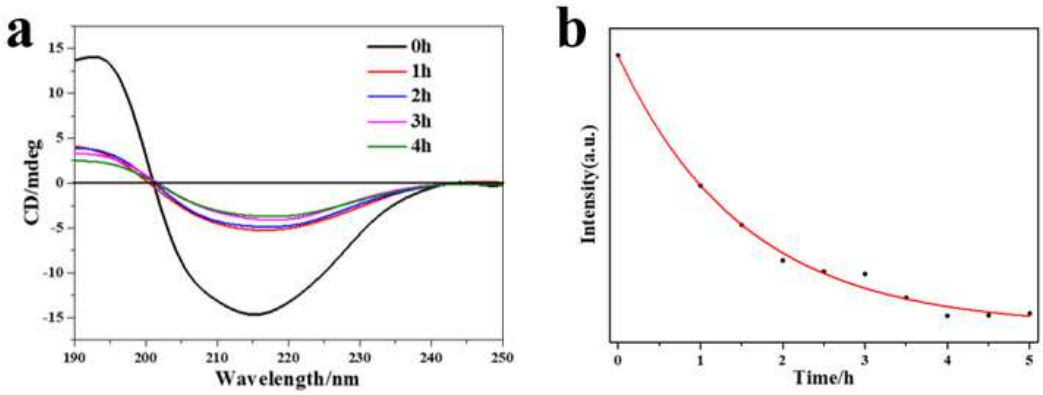

Figure 7. The secondary structure characterization for Aβ(1-40) aggregates during photodegradation; (a) The CD spectra measured by J-815; (b) ThT assay measured by ELASA.

4. Conclusion

In this work, we successfully synthesized the Cu-Cy nanoparticles. Further, we proved that PEG modification can significantly improve the biocompatibility of Cu-Cy. Cu-Cy-PEG presented a high photodegradation efficiency on Aβ(1-40) aggregates under the UV irradiation. AFM images and ThT fluorescence demonstrated most of aggregates were degraded into

nanoparticles. This work presents an important proof that Cu-Cy-PEG can be a potential scavenge reagent for amyloid aggregates in AD therapy.

Reference

[1] Carter J, Lippa C F. β-Amyloid, Neuronal Death and Alzheimer's Disease[J]. Current Molecular Medicine, 2001, 1(6): 733-737.

[2] Nunomura A, Moreira P I, Lee H G, et al. Neuronal Death and Survival Under Oxidative Stress in Alzheimer and Parkinson Diseases[J]. CNS & Neurological Disorders - Drug Targets- CNS & Neurological Disorders), 2007, 6(6): 411-423.

[3] Gwon A R, Park J-S, Park J-H, et al. Selenium attenuates Aβ production and Aβ-induced neuronal death[J]. Neuroscience Letters, 2010, 469(3): 391-395.

[4] Hardy, J. A, Higgins, et al. Alzheimer's disease: The amyloid cascade hypothesis[J]. Science, 1992.

[5] Ow S Y, Dunstan D E J P S. A brief overview of amyloids and Alzheimer's disease[J]. Protein Science, 2015, 23(10): 1315-1331.

[6] Tsatsanis A, Wong B X, Gunn A P, et al. Amyloidogenic processing of Alzheimer's disease β-amyloid precursor protein induces cellular iron retention[J]. Molecular Psychiatry, 2020, 25(9): 1958-1966.

[7] Lee B I, Lee S, Suh Y S, et al. Photoexcited Porphyrins as a Strong Suppressor of β-Amyloid Aggregation and Synaptic Toxicity[J]. Angewandte Chemie International Edition, 2015, 54(39): 11472-11476.

[8] Li Y, Du Z, Liu X, et al. Near-Infrared Activated Black Phosphorus as a Nontoxic Photo-Oxidant for Alzheimer's Amyloid-β Peptide[J]. Small 2019, 15(24): 1901116.

[9] Heo Y, Kim K, Kim J, et al. Near-Infrared-Active Copper Bismuth Oxide Electrodes for Targeted Dissociation of Alzheimer's β-Amyloid Aggregates[J]. ACS Applied Materials & Interfaces, 2020, 12(21): 23667-23676.

[10] Atsumi T, Murata J, Kamiyanagi I, et al. Cytotoxicity of photosensitizers camphorquinone and 9-fluorenone with visible light irradiation on a human submandibular-duct cell line in vitro[J]. Archives of Oral Biology, 1998, 43(1): 73-81.

[11] Casas A, Fukuda H, Di Venosa G, et al. Photosensitization and mechanism of cytotoxicity induced by the use of ALA derivatives in photodynamic therapy[J]. British Journal of Cancer, 2001, 85(2): 279-284.

[12] Otvagin V F, Kuzmina N S, Kudriashova E S, et al. Conjugates of Porphyrinoid-Based Photosensitizers with Cytotoxic Drugs: Current Progress and Future Directions toward Selective Photodynamic Therapy[J]. Journal of Medicinal Chemistry, 2022, 65(3): 1695-1734.

[13] Chen X, Liu J, Li Y, et al. Study of copper-cysteamine based X-ray induced photodynamic therapy and its effects on cancer cell proliferation and migration in a clinical mimic setting[J]. Bioactive Materials, 2022, 7: 504-514.

[14] Chudal L, Pandey N K, Phan J, et al. Copper-Cysteamine Nanoparticles as a Heterogeneous Fenton-Like Catalyst for Highly Selective Cancer Treatment[J]. ACS Applied Bio Materials, 2020, 3(3): 1804-1814.

[15] Kuk S, Lee B I, Lee J S, et al. Rattle-Structured Upconversion Nanoparticles for Near-IR-Induced Suppression of Alzheimer's β-Amyloid Aggregation[J]. Small, 2017, 13(11): 1603139.

[16] Mold M, Ouro-Gnao L, Wieckowski B M, et al. Copper prevents amyloid-β(1-42) from forming amyloid fibrils under near-physiological conditions in vitro[J]. Sci Rep, 2013, 3: 1256.

[17] Pandey N K, Chudal L, Phan J, et al. A facile method for the synthesis of copper-cysteamine nanoparticles and study of ROS production for cancer treatment[J]. Journal of Materials Chemistry B, 2019, 7: 6630-6642.

[18] Ma L, Chen W, Schatte G, et al. A new Cu-cysteamine complex: Structure and optical properties[J]. Journal of Materials Chemistry C, 2014, 2(21): 4239-4246.

[19] Huang X, Wan F, Ma L, et al. Investigation of copper-cysteamine nanoparticles as a new photosensitizer for anti-hepatocellular carcinoma[J]. Cancer Biology & Therapy, 2019, 20(6): 812-825.

[20] Matrana B A, Bordelon W R, Davis D G. Polarography of Copper (II)-(I) Cysteamine-Cystamine Systems[J]. Analytical Letters, 1971, 4(7): 437-444.

[21] Desimone R E, Ontko T, Wardman L, et al. Electron spin resonance study of iron(III) and ruthenium(III) in a trinuclear complex of tris(2-mercaptoethylamine)cobalt(III)[J]. Inorganic Chemistry, 1975, 14(6): 1313-1316.

[22] Ma L, Chen W, Schatte G, et al. A new Cu–cysteamine complex: structure and optical properties[J]. Journal of Materials Chemistry C, 2014, 2(21): 4239-4246.

[23] Vogler A, Kunkely H. Photoluminescence of tetrameric copper(I) iodide complexes solutions[J]. Journal of the American Chemical Society, 1986, 108(23): 7211-7212.

[24] Zulu M M, Lees A J. Multiple-state emission from ligand-bridged tungsten carbonyl [(OC)5W-L-W(CO)5] complexes[J]. Inorganic Chemistry, 1989, 28(1): 85-89.

[25] Kim S, Fujitsuka M, Majima T. Photochemistry of Singlet Oxygen Sensor Green[J]. The Journal of Physical Chemistry B, 2013, 117(45): 13985-13992.

[26] Krajczewski J, Rucińska K, Townley H E, et al. Role of various nanoparticles in photodynamic therapy and detection methods of singlet oxygen[J]. Photodiagnosis and Photodynamic Therapy, 2019, 26: 162-178.

[27] Wang Y, Alkhaldi N D, Pandey N K, et al. A new type of cuprous-cysteamine sensitizers: Synthesis, optical properties and potential applications[J]. Materials Today Physics, 2021, 19: 100435.

[28] Ni J, Taniguchi A, Ozawa S, et al. Near-Infrared Photoactivatable Oxygenation Catalysts of Amyloid

Peptide[J]. Chem, 2018, 4(4): 807-820.

Supplementary Files

This is a list of supplementary files associated with this preprint. Click to download.

- SupportInformation.pdf